Analysis and impact of the Hunga Tonga-Hunga Ha'apai Stratospheric Water Vapor Plume

M. R. Schoeberl & Yi Wang, Science and Technology Corporation, Columbia, MD, USA

R. Ueyama, NASA Ames Research Center, Moffett Field, CA, USA

G. Taha, Morgan State University, Baltimore, MD, USA

E. Jensen, CIRES, Univ. of Colorado, Boulder, CO, USA

W. Yu, Hampton University, Hampton, VA, USA

Corresponding Author: Mark Schoeberl (mark.schoeberl@mac.com)

Key Points

- Hunga Tonga-Hunga Ha'apai eruption produced vertically overlapping but slightly displaced mid-stratospheric enhancements in H_2O and aerosols.
- IR cooling by enhanced H_2O layer explains the observed 4.1 K mid-stratospheric temperature decrease following the eruption.
- A simple model of the eruption H_2O enhancement combined with spreading of the plume explains the observations.

Plain Language Summary

The Hunga Tonga-Hunga Ha'apai submarine volcanic eruption on January 15, 2022, injected up to 150 Tg of water into the stratosphere. A month after eruption, a distinct aerosol and water vapor layer formed in the tropical southern hemisphere (SH) stratosphere. The water vapor layer is slightly displaced above the aerosol layer at 26 km. These two layers continued to persist in the tropical SH stratosphere until the end of June while slowly moving apart in altitude. The isolation of the layers and their separate motion are consistent with our understanding of tropical stratospheric dynamics. A cold temperature anomaly forms coincident with the water vapor layer, which we show to be due to enhanced IR radiative cooling by water vapor. Using a simple model, we show how the water vapor layer forms slightly above the aerosol layer.

Abstract

On Jan. 15, 2022, the Hunga Tonga-Hunga Ha'apai eruption injected SO_2 and H_2O into the middle stratosphere. The eruption produced a persistent mid-stratospheric sulfate aerosol and H_2O layer mostly confined to Southern Hemisphere (SH) tropics (Eq. to 30°S). These layers are still present in the tropics 5 ½ months after the eruption. The SH tropical confinement is simulated using a trajectory model. Measurements following the eruption show that the H_2O layer is slowly rising while the aerosol layer is descending. The H_2O layer's upward movement is consistent with the residual vertical velocity. Gravitationally settling explains the descent of the aerosol layer. A -4K temperature anomaly coincident with the H_2O enhancement is observed and is caused by thermal adjustment to the additional H_2O IR cooling. A simple model of volcanic water injection at the time of the eruption simulates the observed vertical distribution H_2O.

Index Terms

0340 Middle atmosphere dynamics

0341 Middle atmosphere: constituent transport and chemistry

0370 Volcanic effects

1. Introduction

The Hunga Hunga-Tonga Ha'apai (HT) (20.54°S, 178.3°W) submarine volcano violently erupted on Jan. 15, 2022. The volcanic explosivity index (VEI) was 5, comparable to Krakatau eruption in 1883. Since HT was a submarine volcano, it appears to have lofted a significant amount of water into the stratosphere. Indeed, Microwave Limb Sounder (MLS) measurements show that HT water enhancement was quite high relative to SO_2 (Millán et al., 2022) – hereafter M22. The MLS estimated water injection was up to 146 Tg (M22). The eruption plume was detected up to 57 km on January 15, 2022 (Carr et al., 2022; Proud et al., 2022). The Ozone Mapping and Profile Suite – Limb Profiler (OMPS-LP) detected extinction enhancements above 45 km (Taha et al., 2022).

In this paper we will examine at the evolution of the water vapor and aerosol enhancements that followed the HT eruption. M22 noted that the amount of water deposited in the stratosphere by HT was unprecedented in the modern history of volcanic eruption observations. Several MLS water vapor profiles made shortly after the eruption show concentrations exceeding 300 ppmv against a normal stratospheric concentration of ~4 ppmv. As the eruption evolved, MLS water vapor maps show that above about 2 hPa (~43 km), the plume quickly spreads and that the water vapor enhancement disperses. A secondary maximum at about 25 hPa (~26 km) persists (M22). The aerosol field shows similar behavior with rapid dispersal at higher altitudes but persistent high levels of aerosol extinction below ~ 25 hPa (~26 km) (Taha et al., 2022). The aerosol extinction in this layer grows over the 30 days following the eruption presumably due to the conversion of SO_2 to sulfate aerosols (e.g. Zhu et al., 2020).

There are several key questions concerning the HT eruption: Why did the unusual water vapor layer form and persist? How is it related to the aerosol layer? Below we show that the water vapor enhancement overlaps the top of the extinction anomaly, but they are distinct, and furthermore the two enhancements vertically separate over time. We have also discovered a temperature anomaly in the 25-28 km region. We provide an explanation for the temperature anomaly as well as for the formation and evolution of the water vapor and aerosol layers.

2. Data sets

Generally, we use MLS v5 for ozone, temperature and H_2O where the data where the quality and convergence flags are not set. However, the MLS algorithm quality flags and convergence alerts were set for some plume profiles in the week or so after the eruption. However, even with the quality flag and convergence filters set, the data look reasonable and generally agrees with sonde and other validation data so we used the immediate post eruption data. The data quality for the HT anomaly is detailed in M22 and MLS data is described in Livesy et al. (2021). For aerosols, we use OMPS-LP level-2 V2.1 745 nm extinction-to-molecular ratio data (AE) from all three OMPS-LP slits (see Taha et al., 2021). Taha et al. (2022) indicated that the standard V2.1 released data (used in this study) provide the most accurate aerosol retrieval up to 36 km. Thus, we restrict our constituent analysis to below 35 km which contains the main locus aerosol plume (Taha et al. 2022; Fig. 4). The MLS and OMPS-LP extinction data sets are averaged over 4 days and then averaged onto a 5° latitude-longitude grid.

To simulate the dispersal of the water vapor/aerosol plumes, we use the Forward Domain Filling (FDF) trajectory model (Schoeberl et al., 2018) modified to inject a dense uniform column of parcels over the HT location on Jan 15, 2022. This simulation uses MERRA-2 reanalysis winds, temperatures, and heating rates (Gelaro, et al., 2017).

3. Analysis

Figure 1 shows the zonal mean distribution of water vapor and aerosol extinction ratio on Feb 15, 2022, a month after the eruption. The HT aerosol plume reaches 26 km in the region 30°S to about 5°N. The extinction data are quite sensitive to plumes extending outward from the tropics thus tend to show a wider distribution than the water vapor field. The water vapor plume is centered at 26 km and extends up to 30 km in the SH tropics. The water vapor plume mostly overlaps the aerosol plume while extending slightly above it.

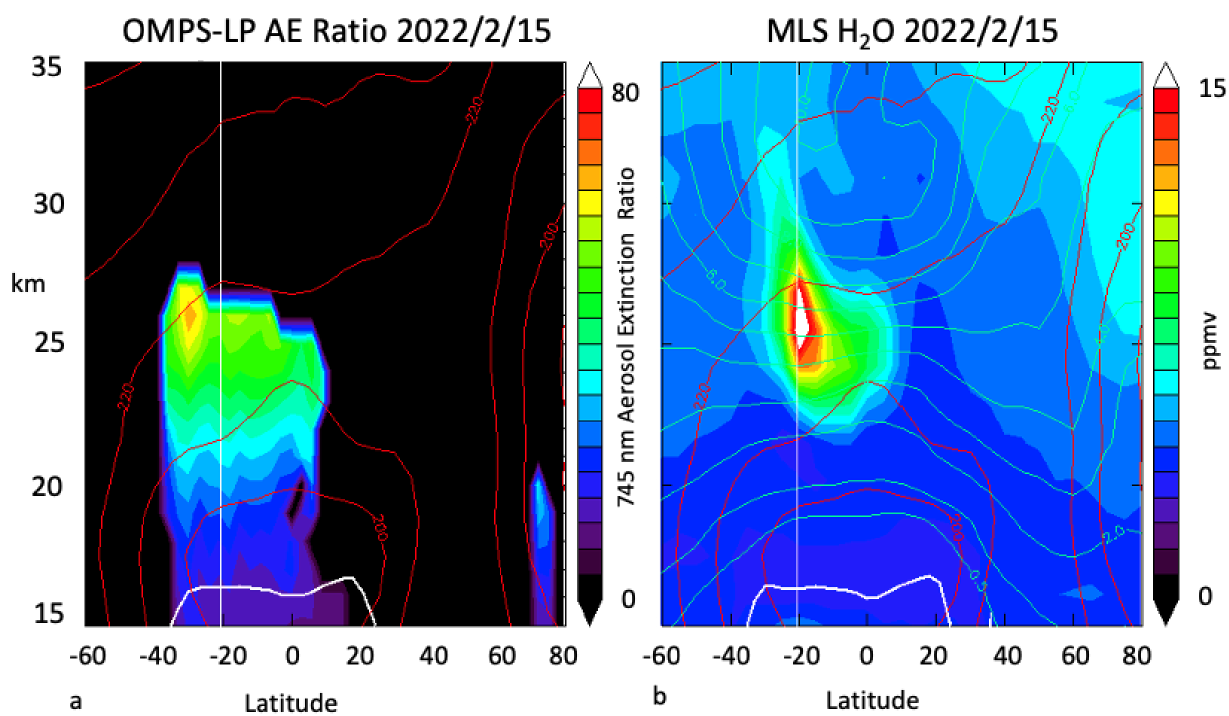

Figure 1 The zonal mean OMPS-LP 745 nm aerosol extinction/ molecular extinction ratio (Part a) and MLS water vapor (ppmv) (Part b) on Feb. 15, 2022. The red contours show the MLS temperature field. The thick white line is the zonal mean tropopause. The green contours are MLS ozone mixing ratio (ppm). The vertical white line denotes the latitude of the HT volcano.

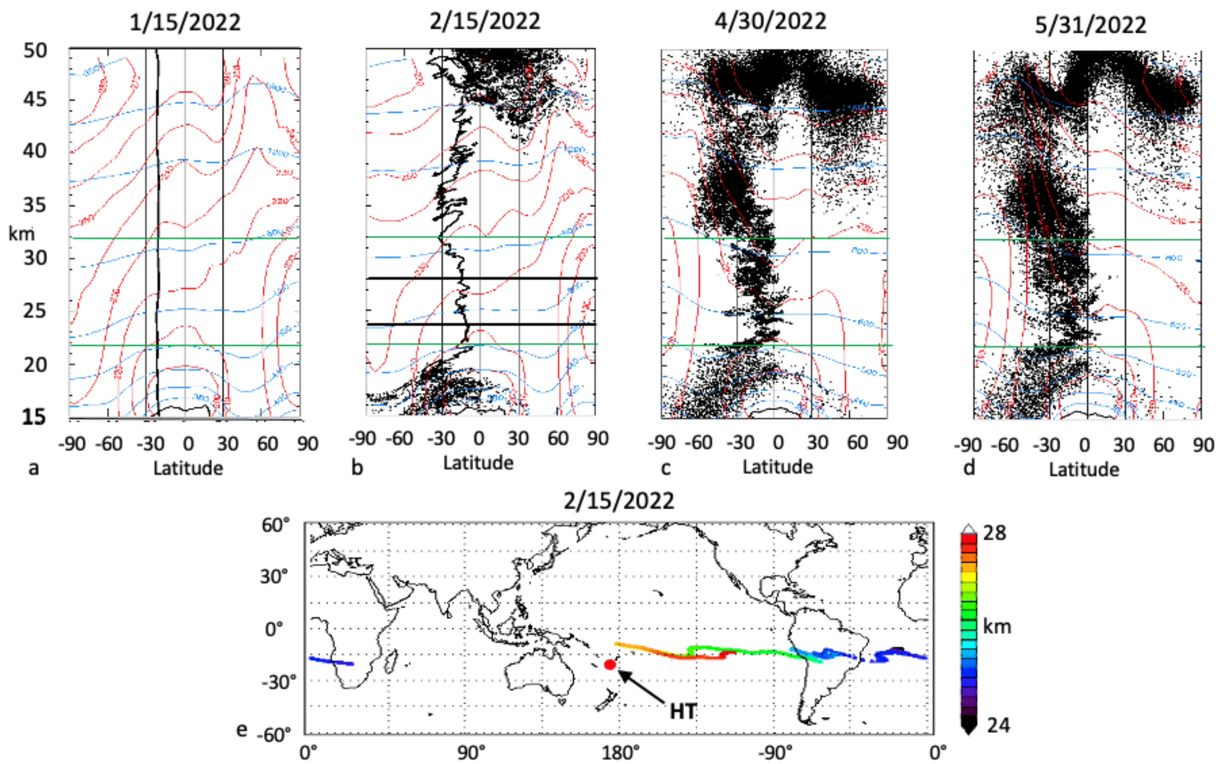

Figure 2 Dispersal of HT plume simulated by the FDF model: (Part a) shows the initial parcel distribution on Jan 15, (Part b) parcel distribution of Feb. 15, 2022, (Part c) shows the distribution at the end of April, and (Part d)shows the distribution at the end of May. Along the bottom (Part e), a map of parcels between 24-28 km with color scale indicating altitude. In Parts a,b,c,d red contours are MERRA-2 temperatures, blue contours are potential temperature. Horizontal green lines show the isolation region 22-32km. Horizontal black lines in Part b indicate the domain in Part e. The red dot locates HT on the map.

Figure 2 shows the dispersal of the plume using the FDF trajectory model. From the initial uniform altitude distribution (Fig. 2a), the plume evolves slowly and is mostly confined to the region between the equator and 30°S in the height range 22-32 km. This confinement is still somewhat evident at the end of April. The isolation of the Northern Hemisphere (NH) tropics from the Southern Hemisphere (SH) tropics in this region was first noted by Stolarski et al. (2014) when analyzing the interhemispheric phasing of the tropical ozone concentration. Below ~20 km parcels are dispersing mostly to the SH extra-tropics along the isentropes. Above about 35 km parcels are also dispersing and drifting poleward together into the SH. At highest altitudes, parcels are moving out of the tropics into the NH extra-tropics.

Timeseries of the zonal mean aerosols and water vapor at 15°S±2.5° are shown in Fig. 3a,b. We also plot the temperature anomaly (Fig. 3c) as a departure of the zonal mean MLS temperature from the 2021-2016 MERRA2 climatology. The perturbation heating rate shown in Fig. 3d is computed using the AER longwave radiative transfer model (Mlawer et al., 1997). The heating rate calculation uses observed MLS ozone, temperature, and water vapor. The heating rate anomaly is computed by fixing the water vapor to the pre-eruption profile and computing the heating rates over the period. We then subtract those heating rates from the heating rates computed using MLS observed water vapor data.

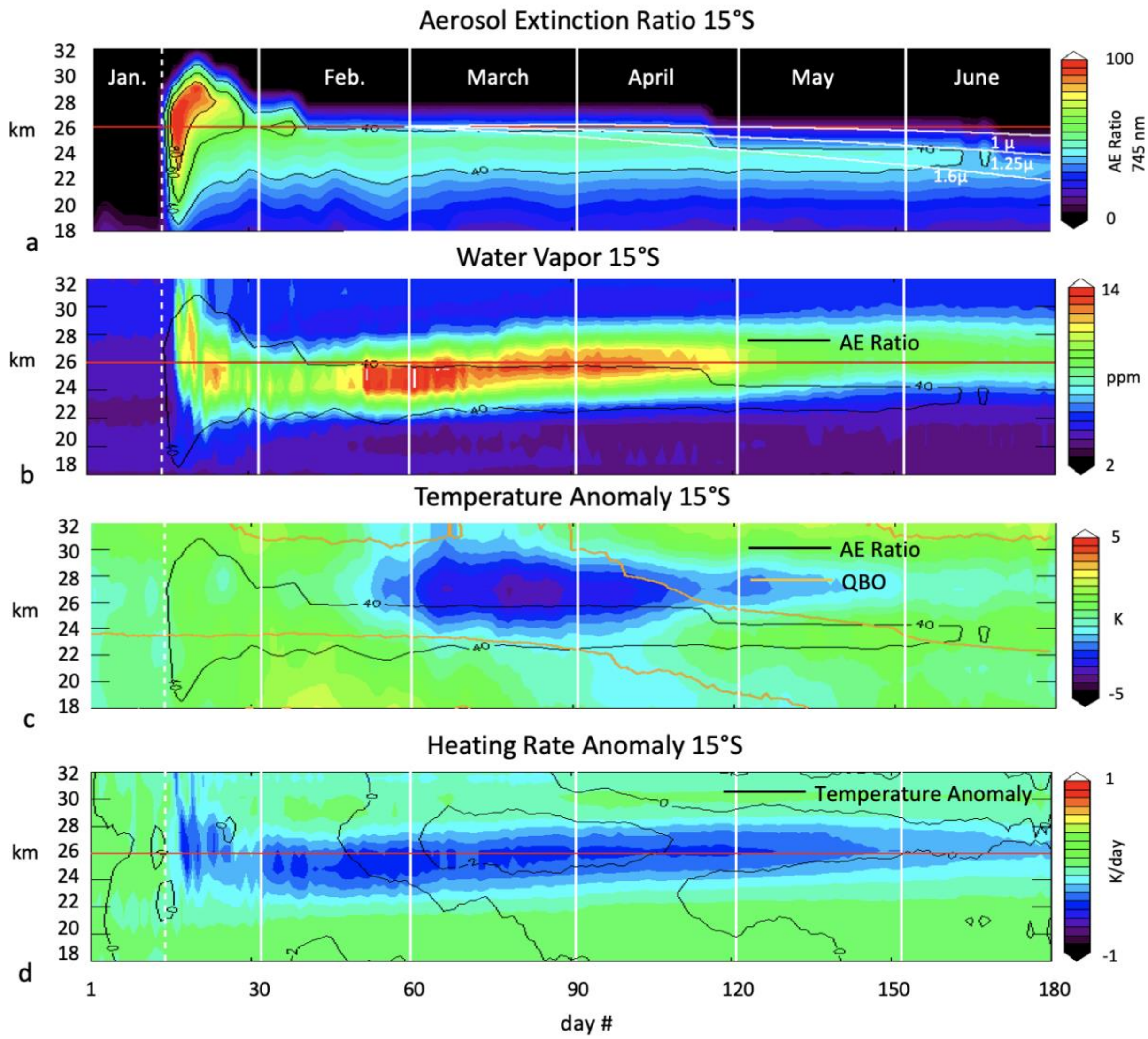

Figure 3 Times series of 2022 aerosol extinction ratio (AE) (Part a), water vapor (Part b), temperature anomaly (Part c), and heating rate anomaly (Part d) at 15°S. Parts b & c show black contours of 40 AE ratio that outline the aerosol anomaly. In Part d, the heating rate anomaly has the Part c temperature contours superimposed. White lines in Part a represent the downward gravitational settling of aerosols of different diameters (µm) as labeled. Orange contours in Part c (QBO) indicates the altitude of the zero zonal wind lines at the equator showing the descent of the QBO. The red line in all parts is at 26 km. Vertical white lines show month boundaries, months labeled in Part a.

Comparing the aerosol extinction field (Fig. 3a) with the water vapor (Fig. 3b), we see that the water vapor anomaly is slowly ascending whereas the aerosol concentration is descending. The simple explanation for this effect is that the water vapor is transported upward with the diabatic circulation that gives rise to the tropical trace gas tape recorders (Schoeberl et al., 2008a) whereas the aerosols are gravitationally settling. The 26 km water vapor anomaly ascent rate is ~2 km over 45 days (after March 1) or ~0.044 km/day. We have computed the residual circulation over the same period, and it averages to 0.045 km/day consistent with the estimate from water vapor. Using w* as the ascent velocity, Fig 3a shows the net settling rate for aerosols with different sizes after day 60. The settling rate is computed from Stokes formulas in Pruppacher et al. (1998). The change in the aerosol height appears to match the settling for aerosol modal diameter of ~1.2 µm. Smaller particles would be carried upward by the circulation into warmer, lower relative humidity environment, and would evaporate (Tsagkogeorgas et al., 2017).

By mid-March, the descending QBO circulation weakens the background upward residual circulation to ~0.02 km/day which slows the ascent of the water vapor anomaly as is evident in Fig. 2b. The equatorial zero wind line altitude is superimposed on Fig. 3c to show the descent (see https://acd-ext.gsfc.nasa.gov/Data_services/met/qbo/qbo.html).

Fig. 3c shows a cold temperature anomaly that begins to appear in early to mid-February, and the anomaly magnitude is consistent with radiosonde measurements (Vömel et al., 2022). This temperature anomaly, which exceeds -4K, is approximately coincident with the change in the cooling rate (Fig. 3d; correlation of r = 0.77 for the period Feb. 15-July 1) due to enhanced water vapor. If we assume in the thermodynamic equation that the temperature change (DT) balances the change radiative heating (ΔH), $\Delta T \sim a\Delta H$, then we compute a Newtonian cooling time scale (a^{-1}) of 3.3 days at 26 km. This time constant is consistent other estimates of the Newtonian cooling rate for this region (e.g. Newman and Rosenfield, 1997). Thus, the temperature changes observed in the mid stratosphere are part of the thermal adjustment to the increased IR cooling, and we expect circulation changes as well (Coy et al., 2022).

Note that volcanic aerosols can heat the stratosphere (Aubry et al., 2021 and references therein) and this heating would oppose the water vapor cooling. Shortly after the eruption, sonde measurements show a < 2K increase in temperatures below 25 km that disappears by early February (Vömel et al., 2022). After February we see no evidence of a temperature change co-located with the aerosol layer probably because the dispersed aerosol layer is too attenuated.

What governs the vertical structure of the water vapor anomaly? To explore this problem, we have constructed a very simple model of the HT plume based on observations. Initially, the eruption is propelled upward by the explosion and latent heat release through condensation of water vapor at lower altitudes. The initial plume temperature is likely well above stratospheric ambient temperatures. Within days to weeks the plume shears out and plume temperature cools to ambient. Estimates of aerosol radiative heating by Silletto et al. (2022) show that longwave aerosol cooling and shortwave aerosol heating nearly cancel leaving water vapor cooling as the major radiative component. We assume, for simplicity, that the amount of water vapor available is now limited by the saturation mixing ratio over ice i.e., excess water forms ice particles that quickly fall out until the relative humidity is reduced to 100%. The falling ice evaporates, saturating any unsaturated layers below. We then assume that the amount of HT water lofted decreases above the eruption top centroid height in mid-February – prior to mid-February the system is still in adjustment (Legras et al., 2022). These two principles define the available water. Based on GOES images, the 16 km volcanic cloud is ~ 500-1000 km in diameter. This area must expand with altitude, to conserve mass. As in Fig. 2e, the eruption cloud stretches out in longitude. Thus, by mid-February MLS zonal mean water vapor is the available water in the eruption cloud reduced by the ratio of the initial eruption cloud area to the tropical zonal mean area.

The model uses the OMPS-LP mid-February aerosol extinction profile (Fig. 1a) to set the eruption top centroid height, $z_{cent,}$; the model assumes the cloud is roughly mixed zonally. We center a vertical Gaussian-type distribution around the centroid. The temperature profile at 20°S is shown in Fig. 4a along with the saturation mixing ratio over ice (Murphy and Koop, 2005). Below the eruption centroid, the ice amount is equal to the saturation mixing ratio; above the centroid, the amount of water available is the saturation mixing ratio decreasing with altitude as $\exp(-(z-z_{cent})^2/2L^2)$ where L=0.65km and z_{cent} = 26 km. We add the observed background pre-eruption zonal mean MLS water vapor profile for realism. Fig. 4b shows the assumed eruption available water vapor profile and relative humidity on Feb 15. The available water reaches 600 ppmv at 26 km. MLS did observe the water vapor mixing ratios over 300 ppm at 26 km Jan. 16 (M22) and there are sonde measurements of even higher mixing ratios in this stratospheric region (Vömel et al., 2022).

The Feb. 15 zonal mean water vapor field (Fig. 4c) is assumed to be 15° wide from 5°S to 20°S and consists of the diluted plume shown in Fig. 3b. Fig. 4c also shows the observed aerosol extinction profile. The aerosol extinction profile is only used to verify the height of the eruption centroid and its width. The water vapor profile shows good agreement with zonal mean MLS data at 15°S. The extension of the water plume above the aerosol plume is also reproduced. The Fig 4c column water vapor mass above 100 hPa is 32.8 Tg; the MLS mass is 31.2 Tg.

In summary, the simple model requires three factors to explain the water vapor anomaly that extends above the aerosol anomaly: (1) the change in the saturation mixing ratio with altitude as controlled by the tropical temperature profile, (2) a decrease in volcanic water injection above the eruption top, and (3) spatial dilution of the eruption plume.

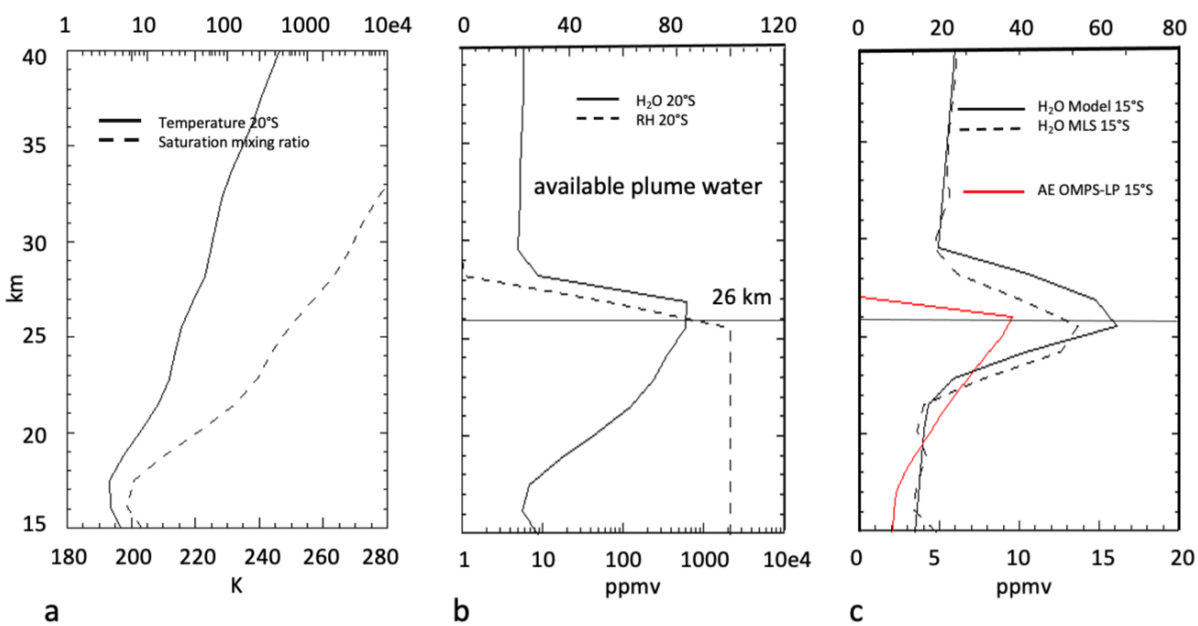

Figure 4 Model of HT water vapor injection. Part a shows Jan 15, 2022 temperature and saturation mixing ratio profile at the location of HT (20°S). Part b shows a model of the eruption

available water vapor to be mixed with the environment, and relative humidity profile, the eruption top is at 26 km. Part c shows the zonal mean aerosol extinction ratio profile for Feb. 15, 2022 (red). Zonal mean water vapor profile (black) for the model and MLS zonal mean water vapor (dashed).

5. Summary and Discussion

The HT volcanic eruption produced stratospheric enhancements of both water and aerosols (sulfate after SO_2 oxidation). Our analysis shows that the aerosol and water vapor enhancements persisted from Jan 15 to July 1, 2022. Between 22-32 km the enhancements are confined mostly to the SH tropics as is evident from observations and consistent with a trajectory analysis. This isolation of the stratospheric SH tropics from the NH tropics is consistent with tropical ozone observations (Stolarski et al., 2014). Below about 20 km, the aerosol observations and trajectory analyses show that aerosols and water mostly disperse out of the SH tropics. The trajectories suggest that most of the aerosols move to the SH with a smaller amount moving into the NH. Above 40 km the trajectory model suggests that eruption material moves into the Northern Hemisphere as part of the cross-hemispheric upper stratospheric circulation (Schoeberl and Strobel, 1978; Holton and Wehrbein, 1980).

By mid-February, the tropical mid-stratosphere aerosol and water vapor enhancements are slightly offset from each other, with the water vapor anomaly about 1 km higher. The two distinct layers continue separate over the 5½ month period following the eruption. The ascent speed of the water vapor anomaly is consistent with the magnitude of the upward branch of the large scale residual circulation. The descent of the aerosol layer is consistent with the gravitational settling of particles ~ 1.2 µm consistent with an independent analysis by Legras et al. (2022). Smaller particles will be carried upward by the circulation and evaporate in the warmer layers above.

Tropical temperatures at 26 km, 15°S show anomalous decreases about a month after the eruption and are coincident with the water vapor enhancement at that altitude. This temperature decrease is also seen in sonde measurements (Vömel et al., 2022). IR radiative transfer computations show that the temperature decrease is correlated with enhanced water vapor IR cooling as might be expected (de F. Forster and Shine, 1999). The short-wave heating and long wave cooling by aerosols appear to roughly cancel (Silletto, 2022). Thus, the temperature change appears to be part of the dynamical response to the increased H_2O IR cooling. The other part of the response will be a circulation adjustment (Coy et al., 2022). The Newtonian cooling rate calculated from observed temperature and cooling rate changes is consistent with previous computations (Newman and Rosenfield, 1997).

To explore the formation of the water vapor anomaly, we use a simple model of the eruption. In the model we define an eruption top altitude, we assume that there is a decreasing amount of water injected above that altitude and the relative humidity below that altitude is 100%. The water vapor then disperses zonally. Our model water vapor matches the zonal mean MLS measurements one month after the eruption and is consistent with the range of MLS H_2O measurements made shortly after the eruption (M22).

Our simple model suggests that even larger water vapor anomalies would have formed if the volcanic eruption had lofted water into higher, warmer stratospheric air. On the other hand, smaller water vapor anomalies would have occurred for lower altitude injections or higher latitude injections into colder stratospheric air. This, along with the fact that most volcanic eruptions in the recent past were not submarine may explain why water vapor enhancements have not been as large in previous eruptions (e.g. St. Helens - Murcray et al., 1981; Calbuco - Sioris et al. 2016; Kasatochi - Schwartz et al., 2013).

Acknowledgements

This work was supported under NASA grant NNX14AF15G, and 80NSSC21K1965. The authors would like to thank Natalya Kamarova for discussions, and the reviewers for excellent suggestions.

Open Research

MERRA-2 Reanalysis data. Gelaro et al. (2017). MERRA-2 data are obtained from the Global Modeling and Assimilation Office (GMAO), *inst3_3d_asm_Cp: MERRA-2 3D IAU State, Meteorology Instantaneous 3-hourly (p-coord, 0.625x0.5L42)*, *version 5.12.4* at https://doi.org/10.5067/WWQSXQ8IVFW8. Data is public, unrestricted access (registration required).

OMPS-LP data, Taha et al. (2021), is available at https://disc.gsfc.nasa.gov/datasets/OMPS_NPP_LP_L2_AER_DAILY_2/summary, DOI: httos://doi.org/10.5067/CX2B9NW6FI27. The algorithm is documented in Taha et al. (2021). Data is public, unrestricted access (registration required).

Aura MLS Level 2 data, Livesey et al. (2021) JPL D-33509 Rev. C, is available at https://disc.gsfc.nasa.gov/datasets?page=1&keywords=AURA%20MLS
The temperature data is available at https://acdisc.gesdisc.eosdis.nasa.gov/data/Aura_MLS_Level2/ML2T.004/
The V4 water vapor data is available at https://acdisc.gesdisc.eosdis.nasa.gov/data/Aura_MLS_Level2/ML2H2O.004/
The V5 water vapor data is available at https://acdisc.gesdisc.eosdis.nasa.gov/data/Aura_MLS_Level2/ML2H2O.005/

References

Aubry, T. J., J. Staunton-Sykes, L. R. Marshall, J. Haywood, N. L. Abraham & A. Schmidt, (2021)/Climate change modulates the stratospheric volcanic sulfate aerosol lifecycle and radiative forcing from tropical eruptions, Nature Comm., 12:4708 https://doi.org/10.1038/s41467-021-24943-7

Carr, J. L., Horvath, A., Wu, D. L., & Friberg, M. D. (2022). Stereo plume height and motion retrievals for the record-setting Hunga Tonga-Hunga Ha'apai eruption of 15 January, Geophys. Res. Lett. https://doi.org/10.1029/2022GL098131

Coy, L., P. Newman, K. Wargan, G. Partyka, S. Strahan, and S. Pawson, (2022), Stratospheric Circulation Changes Associated with the Hunga Tonga-Hunga Ha'apai Eruption, Geophys. Res. Lett., 49, https://www.essoar.org/doi/abs/10.1002/essoar.10512388.1

de F. Forster, Piers M., Shine, Keith P. (1999) Stratospheric water vapour changes as a possible contributor to observed stratospheric cooling. Geophys.l Res. Let., 26 (21). 3309-3312 doi:10.1029/1999gl010487

Gelaro, R., et al. (2017), The Modern-Era Retrospective Analysis for Research and Applications, Version 2 [Dataset], J. Climate, 30, 5419-5454, https://doi.org/10.1175/jcli-d-16-0758.1.

Holton, J. R. and W. M. Wehrbein (1980), A numerical model of the zonal mean circulation of the middle atmosphere, Pure and Appl. Geophys., 119, 284-306.

Legras, B., C. Duchamp, P. Sellitto, A. Podglajen, E. Carboni, R. Siddans, J.-U. Groob, S. Khaykin, F. Ploeger, The evolution and dynamics of the Hunga Tonga plume in the stratosphere. Atmos. Chem. Phys, https://doi.org/10.5194/egusphere-2022-517.

Livesey, N., Read, W.G., Wagner, P.A., Froidevaux, L., Santee, M.L., Schwartz, M.J. et al. (2021), Earth Observing System (EOS) Aura Microwave Limb Sounder (MLS) version 5.0x level 2 and 3 data quality and description document, JPL D-105336 Rev A. https://mls.jpl.nasa.gov/data/v5-0_data_quality_document.pdf

Millán, L. et al., (2022). The Hunga Tonga-Hunga Ha'apai Hydration of the Stratosphere, Geophysical Research Letters. 49, e2002GL099381,https://doi.org/10.1029/2022GL099381

Mlawer, E.J., S.J. Taubman, P.D. Brown, M.J. Iacono and S.A. Clough: RRTM, a validated correlated-k model for the longwave. *J. Geophys. Res*., **102**, 16,663-16,682, 1997.

Newman, P. A. and J. E. Rosenfield (1997). Stratospheric thermal damping times, Geophys. Res. Lett., 24, 433-436.

Murcray, D. G., F. J. Murcray, D. B. Barker, and H. J. Mastenbrook (1981), Changes in stratospheric water vapor associated with the Mount St. Helens eruption, Science, 211, 823–824.

Murphy, D. M. and T. Koop (2005), Review of the vapour pressures of ice and supercooled water for atmospheric applications, Quart. J. Royal Met. Soc, 131, 1539-1565.

Proud, S. R., Prata, A., & Schmauss, S. (2022). The January 2022 eruption of Hunga Tonga-Hunga Ha'apai volcano reached the mesosphere. Earth and Space Science Open Archive, 11. https://doi.org/10.1002/essoar.10511092.1 doi: 10.1002/essoar.10511092.1

Pruppacher, H. R., J. D. Klett & P. K. Wang (1998). *Microphysics of Clouds and Precipitation*, 28:4, 381-382, doi: 10.1080/02786829808965531

Schoeberl, M. R. and D. F. Strobel, (1978). The Zonally Averaged Circulation of the Middle Atmosphere, *J. Atmos. Sci.*, **35**, 577-591.

Schoeberl, M. R. et al., (2008a) QBO and annual cycle variations in tropical lower stratosphere trace gases from HALOE and Aura MLS observations, J. Geophys. Res, VOL. 113, D05301, https://doi.org/10.1029/2007JD008678

Schoeberl, M. R., A. R. Douglass, R. S. Stolarski, S. Pawson, S. E. Strahan, and W. Read (2008b), Comparison of lower stratospheric tropical mean vertical velocities, J. Geophys. Res., 113, D24109, https://doi.org/10.1029/2008JD010221

Schoeberl, M. R., Jensen, E. J., Pfister, L., Ueyama, R., Avery, M., & Dessler, A. E. (2018), Convective hydration of the upper troposphere and lower stratosphere, J. of Geophys. Res.: Atmospheres, 123, 4583–4593, https://doi.org/10.1029/2018JD028286.

Schwartz, M. J., W. G. Read, M. L. Santee, N. J. Livesey, L. Froidevaux, A. Lambert, and G. L. Manney (2013), Convectively injected water vapor in the North American summer lowermost stratosphere, Geophys. Res. Lett., 40, 2316–2321, doi:10.1002/grl.50421.

Silletto, P., A. Podglagen, R. Belhadji, M. Boichu, E. Carboni, J. Cuesta, C. Duchanp, C. Kloss, R. Siddans, N. Begue, L. Blarel, F. Jegou, S. Khaykin, H-B. Renard, and B. Legras, (2022), The unexpected radiative impact of the Hunga Tonga eruption of January 15, 2022, Research Square (preprint), https://doi.org/10.21203/rs.3.rs-1562573/v1

Sioris, C. E., A. Malo, C. A. McLinden, and R. D'Amours (2016), Direct injection of water vapor into the stratosphere by volcanic eruptions, Geophys. Res. Lett., 43, 7694–7700, doi: 10.1002/2016GL069918.

Stolarski, R. S., D. W. Waugh, L. Wang, L. D. Oman, A. R. Douglass, and P. A. Newman (2014), Seasonal variation of ozone in the tropical lower stratosphere: Southern tropics are different from northern tropics, J. Geophys. Res. Atmos., 119, 6196–6206, doi:10.1002/2013JD021294.

Taha, G., R. Loughman, T. Zhu, L. Thomason, J. Kar, L. Rieger, and A. Bourassa (2021), OMPS LP Version 2.0 multi-wavelength aerosol extinction coefficient retrieval algorithm, Atmos. Meas. Tech., 14, 1015–1036, https://doi.org/10.5194/amt-14-1015-2021

Taha, G., R. Loughman, P. Colarco, T. Zhu, L. Thomason, G. Jaross (2022), Tracking the 2022 Hunga Tonga-Hunga Ha'apai aerosol cloud in the upper and middle stratosphere using space-based observations, Geophysical Research Letters. (submitted).

Tsagkogeorgas et al. (2017), Evaporation of sulfate aerosols at low relative humidity, Atmos. Chem Phys, 17,8923-8938, https://doi.org/10.5194/acp-17-8923-2017.

Vömel, H., S. Evan, and M. Tully (2022), Water vapor injection into the stratosphere by Hunga Tonga-Hunga Ha'apai, Science, 377,1444-1447

Zhu, Y., Toon, O. B., Jensen, E. J., Bardeen, C. G., Mills, M. J., Tolbert, M. A., Yu, P., and Woods, S.: Persisting volcanic 715 ash particles impact stratospheric SO_2 lifetime and aerosol optical properties, Nat. Comm., 11, 4526, https://doi.org/10.1038/s41467-020-18352-5, 2020.